ACS OMEGA

Open Access

http://pubs.acs.org/journal/acsodf

Article

Hydrophobicity-Driven Disruption Mechanism in Kindlin-3 Induced by Leukocyte Adhesion Deficiency Mutation

Xianwen Luo, Quhuan Li,* and Fengxia Zhang*

Cite This: *ACS Omega* 2025, 10, 16396−16409

Read Online

ACCESS | Metrics & More | Article Recommendations | Supporting Information

ABSTRACT: Leukocyte adhesion deficiency type III (LAD-III) is caused by amino acid mutations in Kindlin-3, which result in integrin activation defects. The QW motif in the Kindlin family is particularly important for integrin activation, and the Q595P mutation in the QW motif of Kindlin-3 leads to LAD-III. However, the molecular mechanisms underlying this disruption remain unclear. In this study, we employed molecular dynamics (MD) and steered MD simulations to investigate how the pathogenic Q595P mutation in Kindlin-3 alters its interaction with β1-integrin under physiological conditions. Our results show that the Q595P mutation induces conformational changes in neighboring residues, leading to a reduction in binding affinity, specificity, and mechanical strength, primarily driven by hydrophobic changes. Specifically, the Q595P mutation disrupts the torsional dynamics of residues at the Kindlin-3 binding interface by disturbing the hydrophobic environment, weakening the hydrogen bonds that are essential for stabilizing the Kindlin-3/β1-integrin interaction under both forceful and nonforceful conditions. Additionally, it enhances nonspecific hydrophobic interactions on nonbinding surfaces, further destabilizing the overall binding. These findings provide important insights into the molecular mechanisms by which pathogenic mutations in conserved regions of Kindlin-3 lead to integrin activation defects and contribute to the pathogenesis of LAD-III.

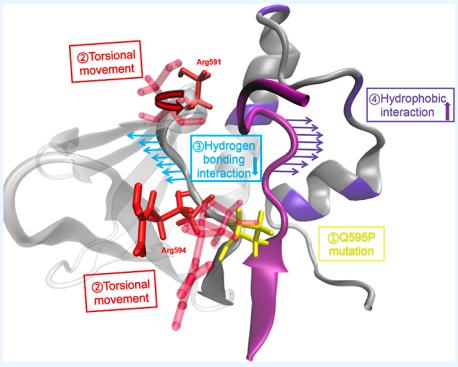

INTRODUCTION

Leukocyte trafficking to the sites of injury or infection involves several processes, including rolling, adhesion, stable adhesion, crawling, and migration.[1] Among these processes, the interaction between adhesion molecules on endothelial cells and integrins on leukocytes mediates both the stable adhesion and transendothelial migration of leukocytes.[2] Integrin activation is a crucial event in leukocyte inflammatory responses during inflammation.[3] Kindlins are key positive regulators of integrin activation. Specifically, they interact with the cytoplasmic tail of integrins to facilitate leukocyte adhesion and migration.[4]

Kindlins are a family of evolutionarily conserved focal adhesion proteins that play crucial roles in integrin activation and cell-extracellular matrix adhesion.[4−6] The structural hallmark of Kindlins is the FERM (protein 4.1, ezrin, radixin, moesin) domain, which includes the F0, F1, F2, and F3 subdomains.[7,8] The F3 subdomain contains a phosphotyrosine-binding (PTB) domain to which Kindlins bind the membrane-distal tail NxxY motif of β integrin[9−11] to coactivate integrins in conjunction with talins.[9,12] The Kindlin family of vertebrates comprises three members: Kindlin-1, -2, and -3 (also known as FERMT1, FERMT2, and FERMT3).[13] Kindlin-1 and -2 are widely expressed in both mouse and human tissues, whereas Kindlin-3 expression is restricted to hematopoietic tissues.[7,14] The normal interaction between Kindlins and integrins is essential for integrin activation.[10,15] Studies have shown that mutations in individual residues at the binding interface, which impart hydrophobic properties, prevent Kindlins from localizing to focal adhesions, leading to abnormal integrin activation and even resulting in associated diseases.[11,16] Mutations in Kindlin-1 cause Kindler syndrome (KS), which is characterized by skin abnormalities including blistering and atrophy, and an increased risk of developing squamous cell carcinomas.[17,18]

Mutations in Kindlin-3 result in leukocyte adhesion deficiency type III (LAD-III),[19−21] which is characterized by Glanzmann thrombasthenia-like bleeding and life-threatening infections similar to LAD-I.[22] However, unlike those with Glanzmann thrombasthenia and LAD-I, patients with LAD-III have normal integrin expression but have activation defects in the β1, β2, and β3 integrins in platelets, neutrophils, and lymphocytes.[23,24] These mutations in Kindlins that cause diseases involve single amino acid changes, some of which result from alterations in the hydrophobicity or hydrophilicity of the amino acids.[25,26] However, it remains unclear how these

Received: December 2, 2024
Revised: January 27, 2025
Accepted: April 14, 2025
Published: April 18, 2025

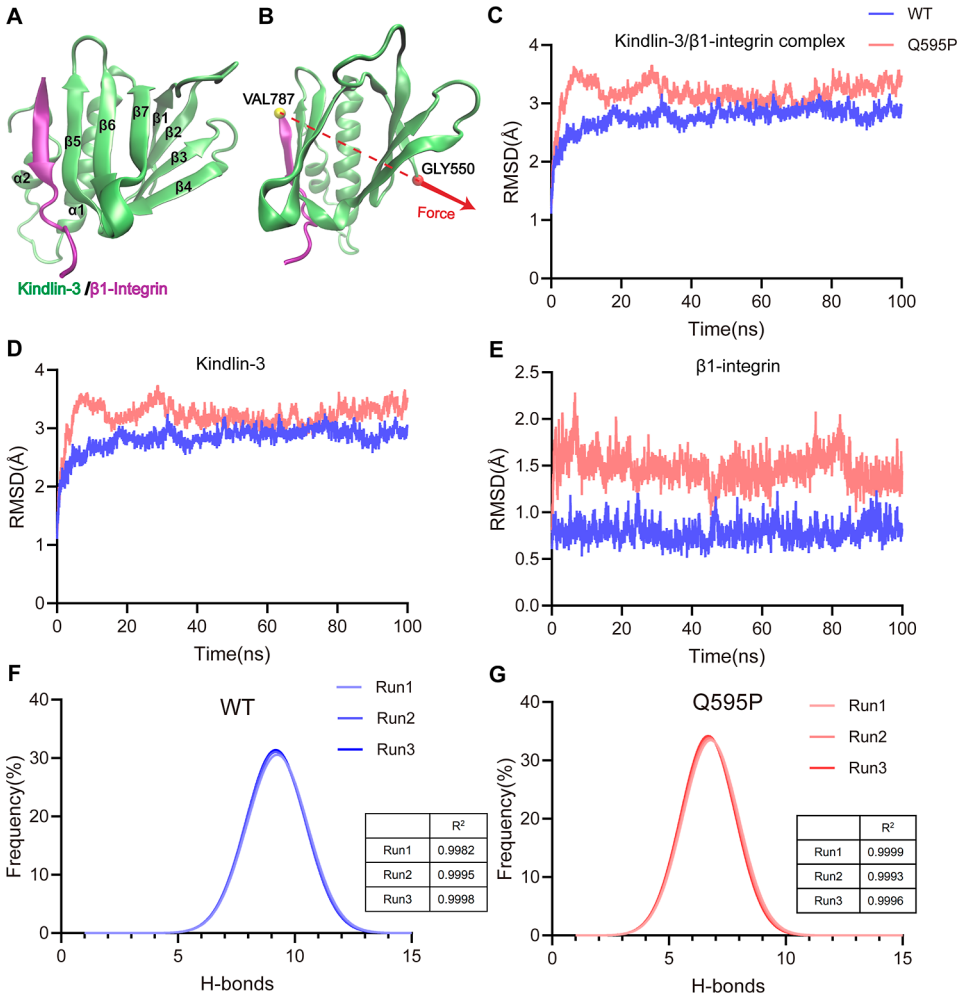

Figure 1. Structural stability of the Kindlin-3/β1-integrin complex. (A) Crystal structure of the Kindlin-3/β1-integrin complex. The Kindlin-3 F3 domain consists of two α-helices and seven β-sheets, and β integrin binds to the $\alpha\beta$-groove formed by the α1-helix and β5-sheet. The β5-sheet constitutes the primary binding interface. (B) The diagram illustrates the exerted force in SMD simulation. The yellow ball represents the fixed Cα atom of Val787, and the red ball represents the pulled Cα atom of Gly550, with the red arrow indicating the stretching direction. (C) Time profile of the Cα RMSD of the Kindlin-3/β1-integrin complex. (D) Time profile of the Cα-RMSD of Kindlin-3. (E) Time profile of the Cα-RMSD of β1-integrin. Each of the time profiles presents an average of results based on three independent runs. (F,G) Distribution of NHB values of the WT (F) and the Q595P mutant systems (G). Gaussian fits exhibit high R^2 values (>0.98), signifying that the conformational space of the complex sampled in equilibrium is quasi-complete across three independent runs.

single amino acid changes affect Kindlin-mediated integrin activation. Therefore, investigating the effects of individual amino acid changes on the binding of Kindlins to integrins at the atomic level may provide valuable insights into this process.

The Gln595 is an amino acid in the highly conserved QW motif of the Kindlin family and is found in the F3 subdomain of Kindlin-3.[13] Mutation of the Gln595 residue to Pro595 contributes to LAD-III.[11,25] Mutations at this site in Kindlin proteins disrupt the interaction between Kindlin and integrin, impairing focal adhesion formation.[11,27] This emphasizes the critical role of this residue in mediating the Kindlin/integrin interaction. Moreover, Kindlin-3 is a mechanosensitive protein that binds to F-actin and transmits mechanical signals from the cytoskeleton to activate integrins.[28] However, studies on mutations at the conserved and pathogenic Gln595 site in the Kindlin family have not yet clarified the molecular details of how the mutation in Kindlin-3 affects its interaction with integrin β. Thus, the molecular mechanism underlying the Q595P mutation in Kindlin-3 and its interaction with integrin β remains unclear.

Molecular dynamics (MD) simulations are widely used to yield detailed insights into the kinetics, structure, and energy information of both free and ligated proteins.[29] This methodology is preferred for investigating the relationship between protein structure and function.[30] In this study, we applied MD and steered MD (SMD) simulations to investigate how the Q595P mutation in Kindlin-3 affects its interaction with β1-integrin. By examining the structural and dynamic changes induced by this mutation, we aim to provide a molecular framework for understanding how hydrophobicity-driven mutations broadly influence Kindlin/integrin interactions. Our findings not only elucidate the potential pathological mechanisms underlying LAD-III but also highlight the potential of MD simulations as a tool for exploring mutation-induced changes in integrin-related diseases, offering insights into the development of targeted therapeutics.

MATERIALS AND METHODS

System Setup. MD simulations with two simulation systems, the wild-type (WT) and Q595P mutant F3 domain

https://doi.org/10.1021/acsomega.4c10930
ACS Omega 2025, 10, 16396−16409

(residues Gly550-Phe663) of Kindlin-3 (PDB ID: 6V9G) in complex with the tail of the β1-integrin (residues Val787−Gly797), were performed. The structure of the Q595P mutant F3 domain was modeled by mutating Gln595 into Pro595 in the WT F3 domain using the "mutate residue" plugin in the visual MD (VMD 1.9.3) software.[31,32] The WT Kindlin-3/β1-integrin complex was constructed by docking the WT F3 domain of Kindlin-3 with β1-integrin (extracted from the Kindlin-2/β1 complex, PDB ID: 5XQ0) using the HADDOCK 2.4 server.[33] The Q595P mutant Kindlin-3/β1-integrin complex was constructed in the same way. Docking sites were chosen based on the top 10 interacting residues ranked by their interaction indices from equilibrium simulations of the Kindlin-2/β1 complex (Table S1). Both the WT and Q595P mutant systems were solvated in TIP3P water by using VMD 1.9.3, with a solvation box extending 15 Å beyond the maximum x, y, and z coordinates of the protein. The systems were neutralized with 150 mM NaCl to mimic the physiological conditions. The total number of atoms in the solvated WT and Q595P mutant systems were 34,469 and 34,139, respectively.

MD Simulations. The flowchart of this study is shown in Figure S1. All-atom MD simulations were conducted using NAMD 2.14 software[34] with the CHARMM36 force field,[35] including CMAP corrections for the protein backbone. Visualization, mutation, and structural analyses were performed using VMD 1.9.3 and PyMOL 2.6.[36] Energy minimization for the WT system was performed in three stages: (1) 15,000 steps with the protein backbone fixed; (2) 15,000 steps with the backbone restrained; and (3) 15,000 steps with all atoms free. The Q595P mutant system was subjected to a four-step minimization process. In the first step, all atoms except the mutated residue were fixed to optimize the structure at the mutation site. The subsequent steps mirrored those of the WT protocol. The minimized systems were gradually heated from 0 to 310 K. Each system underwent three runs of equilibration at 310 K and 1 atm, with each run lasting 100 ns, the equilibrated structure from the 100 ns equilibrium phase was selected as the initial conformation, and a subsequent 100 ns *NPT* simulation was performed for further conformational analysis. Periodic boundary conditions were implemented in all directions, and the particle mesh Ewald method was employed with a maximum grid spacing of 1 Å.

To assess the mechanical strength under an applied force and the conformational changes in the complexes, we conducted a force-ramp SMD simulation[37−39] on the equilibrated system. The force-ramp simulation allowed us to stretch the complex and observe the dissociation process, thereby evaluating the mechanical stability and binding affinity.[40] In the force-ramp MD simulation, in order to simulate the mechanical forces experienced by Kindlin-3 under physiological conditions and prevent nonspecific deformations during the force application process, the C_α atom of residue Val787 at the N-terminus of β1-integrin was fixed, and the C_α atom of residue Gly550 at the N-terminus of the Kindlin-3 F3 domain was pulled along the axis connecting the steered and fixed atoms (Figure 1B). The virtual spring connecting the steered atom to the dummy atom had a spring constant of 13.90 pN/Å. Based on previous studies[41] and our exploration of the stretching velocity in this research (Figure S2), the complex was pulled for 50 ns with a time increment of 2 fs and a pulling velocity of 1 Å/ns. Each system was subjected to three independent pulling simulations to ensure reproducibility.

Data Analysis. Molecular visualization and data analysis were conducted by using the VMD software and TCL scripts. To assess conformational changes and hydrophobic core exposure, the C_α root-mean-square deviation (RMSD) and solvent-accessible surface area (SASA; using a 1.4 Å probe radius) of the Kindlin-3/β1-integrin complex were measured for each simulation, and the hydrogen bonds (H-bonds) at the binding interface were calculated using a donor−acceptor distance cutoff of 3.5 Å and a donor-hydrogen-acceptor angle cutoff of 30°. The binding free energy of the Kindlin-3/β1-integrin complex was evaluated using the molecular mechanics Poisson−Boltzmann surface area (MMPBSA) method.[42−44] The binding free energy of the complex was calculated using the equation: $\Delta G_{bind} = \Delta G_{complex} - (\Delta G_{receptor} + \Delta G_{ligand})$ (1), each term on the right-hand side of eq 1 is computed using the following formula: $\Delta G_{bind} = \Delta E_{MM} + (\Delta G_{solve,polar} + \Delta G_{solve,nonpolar}) - T\Delta S(2)$, where ΔE_{MM} is the gas-phase interaction energy between the complex in a vacuum, $\Delta G_{solve,polar}$ is the polar solvation energy, and $\Delta G_{solve,nonpolar}$ is the nonpolar solvation energy, which is proportional to the SASA and reflects the influence of hydrophobic effects. $\Delta G_{solve,polar}$ was calculated using the following equation: $\Delta G_{solve,polar} = \gamma \times SASA + \beta$ (3), where γ = 0.00542 kcal/mol per Å^2 and β = 0.92 kcal/mol.[45,46] Additionally, $T\Delta S$ is the change in the configurational entropy. Additionally, the dissociation probability (P_D), a parameter indicating the likelihood of ligand dissociation from the receptor, was used to evaluate receptor−ligand binding affinity.

A hydrogen-bonding event occurred once the donor−acceptor distance and the donor-hydrogen-acceptor angle were less than 3.5 Å and 30°, respectively. An occupancy (or survival ratio) of a hydrogen bond was measured by the fraction of bond survival time in the simulation period. Similarly, we quantified the hydrophobic interactions at the binding interface using hydrophobic occupancy, defined as the fraction of hydrophobic contacts during the simulation period. The H-bond network at the protein-binding interface was analyzed using the residue interaction index (P_{ij}), and detailed descriptions of the P_D and P_{ij} calculations were described in our previous work.[38,41]

To investigate major conformational changes within the Kindlin-3/β1-integrin complex, we utilized the GeoStas function from the Bio3D 2.4 package.[47,48] The simulated trajectory was analyzed to obtain the allosteric motion similarity matrix (AMSM) and first principal component (PDB file). These results were visualized by using PyMOL software. Furthermore, the differences in torsional angle between the WT and Q595P mutant systems were calculated using the torsion.xyz function from the same package to highlight residues with significant conformational changes during the simulation.[37] In the SMD, the mechanical strength of the receptor−ligand was evaluated by measuring the maximum rupture force, rupture time, and accumulated stress.

Statistical Analysis. Statistical differences between the groups were assessed using an unpaired two-tailed Student's t test. P-values < 0.05 were considered statistically significant.

RESULTS

Conformational Stability of the Kindlin-3/β1-Integrin Complex at Equilibrium. Three independent 100 ns equilibrium simulations were performed for the Kindlin-3/

https://doi.org/10.1021/acsomega.4c10930
ACS Omega 2025, 10, 16396−16409

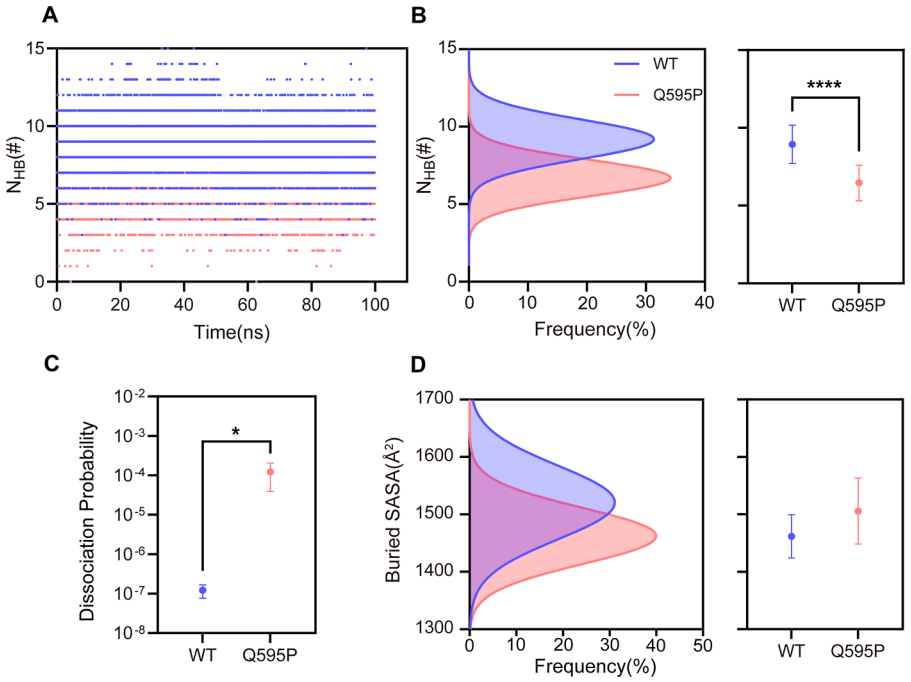

Figure 2. Q595P mutation reduces binding affinity and specificity. (A,B) Time courses (A), Gaussian distribution curves, and averages of the number of H-bonds (B) at the binding interface are shown. Three runs were conducted for the WT and Q595P mutant systems. The mean number of H-bonds is 8.85 ± 0.14 for the WT system and 6.26 ± 0.31 for the Q595P mutant system. (C) Plot of dissociation probabilities. The dissociation probability for the Q595P mutant system was (1.46 ± 0.75) × 10^{-4}, which is higher than that of the WT system [(1.21 ± 1.19) × 10^{-7}]. (D) Gaussian distribution curves and average buried-SASA values. The buried-SASA reached 1505.74 ± 46.90 Å^2 for the Q595P system, which is higher than that of the WT system (1461.62 ± 30.68 Å^2). Statistical significance was indicated by $p < 0.05$ (*) and $p < 0.0001$ (***) based on unpaired two-tailed Student's t test. All data shown are means ± SD, $n = 3$.

Table 1. Binding Free Energies of the Kindlin-3/β1-Integrin Complex Calculated Using the MMPBSA Method (Unit: kcal/mol)[a]

system	ΔE_{MM}	ΔG_{polar}	$\Delta G_{nonpolar}$	ΔG_{bind}
WT	−215.61 ± 22.82	41.76 ± 9.39	−8.66 ± 0.25	−182.51 ± 24.14
Q595P	−150.83 ± 32.45	31.94 ± 4.37	−8.73 ± 0.25	−127.61 ± 19.55

[a]Note: all data shown are means ± SD, $n = 3$.

β1-integrin complex (Figure 1A,B). To assess conformational stability, RMSD values were calculated for both the WT and Q595P mutant systems as well as for the individual Kindlin-3 and β1-integrin proteins. The radii of gyration (R_{gyr}) and solvent-inaccessible surface areas (buried-SASA) of the complexes were measured. The RMSD values of the Kindlin-3/β1-integrin complex (Figures 1C and S4A,B), Kindlin-3 (Figure 1D), and β1-integrin (Figure 1E) in the Q595P mutant system were higher than those of the WT system, indicating that the Q595P mutation increased conformational instability. The R_{gyr} (Figure S3A) and buried-SASA (Figures S3B and S4C,D) values indicated that the complex reached a stable state quickly. Fluctuations in the RMSD and R_{gyr} values stabilized to within 1 Å after 20 ns, confirming the reliability of the docking results. The hydrogen bonds (H-bonds) at the binding sites followed a Gaussian distribution (Figures 1F,G, S4E,F, and S5). Based on the fact that hydrogen bond interactions are the main interactions mediating the binding of the complexes in our system, the high R^2 values (>0.98) of the fitting results for the WT and Q595P mutant systems suggested that the conformational space of the complex samples in the equilibrium was quasi-complete. This confirmed the stability of the simulation system, which enabled detailed subsequent analysis and suggested that the Q595P mutation may alter the overall structure of the complex.

Q595P Mutation Reduces Binding Affinity and Specificity of the Complex. To assess the impact of the Q595P mutation of the complex on the binding affinity, we analyzed the number of H-bonds at the binding interface, dissociation probability, and buried SASA of both systems during the simulation. These results demonstrated that the Q595P mutation reduced the number of H-bonds at the binding interface (Figure 2A,B) and increased the probability of dissociation (Figure 2C), indicating a reduction in binding affinity. Unexpectedly, the buried-SASA values increased slightly after inducing the mutation (Figure 2D), suggesting expansion of the binding interface. To further evaluate changes in binding affinity due to the mutation, the MMPBSA method was applied to calculate binding free energy.[42] This approach integrates molecular mechanical energy terms with hydrophobic effects and offers a comprehensive assessment of the binding affinity. The calculations indicated that molecular mechanical energy (E_{MM}) increased significantly after inducing the Q595P mutation (from −215.61 kcal/mol to −150.83 kcal/mol); polar solvation energy (G_{polar}) decreased (from 41.76 to 31.94 kcal/mol); and nonpolar solvation energy ($G_{nonpolar}$) showed almost no change, indicating that the effect

https://doi.org/10.1021/acsomega.4c10930
ACS Omega 2025, 10, 16396−16409

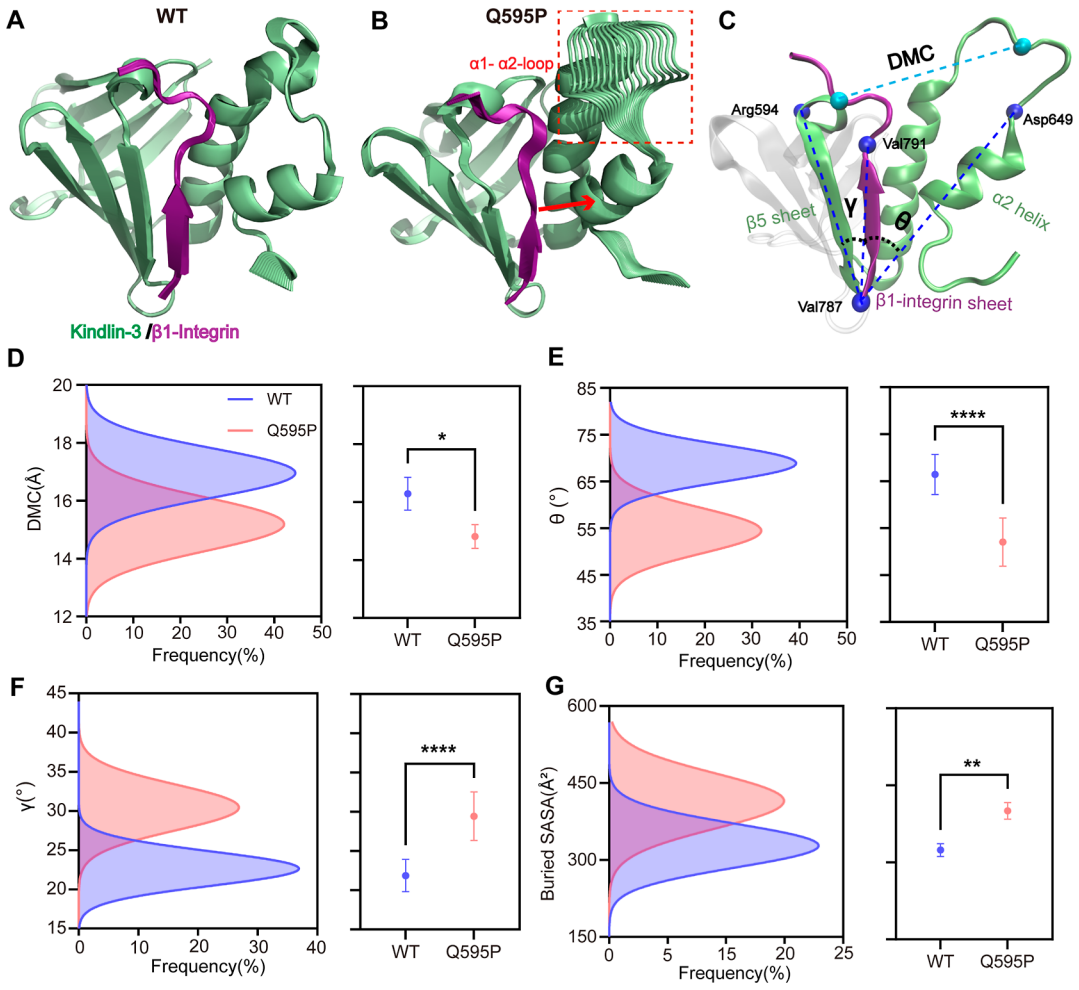

Figure 3. Conformational changes induced by the Q595P mutation. (A) Rigid structural core schematic for the WT system. The WT system displays high overlap, indicating greater conformational stability during the simulation. (B) Rigid structural core schematic for the Q595P mutant system. The α1-α2 loop of Kindlin-3 shows poor overlap, indicating reduced conformational stability. (C) Diagram of centroid distance (DMC) between the β1-integrin loop and the α1−α2 loop of Kindlin-3, including angles θ between the β1-integrin sheet and α2 helix and γ between the β1-integrin sheet and the β5 sheet of Kindlin-3. (D) Changes in the DMC values for the WT and Q595P mutant systems. The DMC values are 16.29 ± 0.46 Å for WT and 14.81 ± 0.33 Å for Q595P. (E) Changes in the θ angle for the WT and Q595P mutant systems. The θ angle is 66.77 ± 5.46 for WT and 51.68 ± 2.55 for Q595P. (F) Changes in the γ angle for the WT and Q595P mutant systems. The γ angle is 21.87 ± 1.61 for WT and 29.44 ± 1.64 for Q595P. (G) Changes in the average buried-SASA values between the β1-integrin loop and the α1−α2 loop of Kindlin-3. The Q595P mutant system buried-SASA reached 400.29 ± 35.16 Å^2, which was higher than that of the WT system (324.00 ± 10.22 Å^2). Statistical significance was indicated by $p < 0.05$ (*), $p < 0.01$ (**), and $p < 0.0001$ (***) based on unpaired two-tailed Student's t test. All data shown are means ± SD, $n = 3$.

of the solvent on the hydrophobic residues of these two systems is essentially the same. Overall, G_{bind} values indicated that the Q595P mutation increased the binding free energy of the Kindlin-3 and β1-integrin complex (Table 1), suggesting a reduction in binding affinity. Our results showed that a slight increase in hydrophobic interactions did not fully compensate for the loss of key specific interactions. Thus, the Q595P mutation decreases the binding affinity and specificity of the complex.

Conformational Changes Induced by the Q595P Mutation in the Kindlin-3/β1-Integrin Complex. The mutation-related reduction in β1-integrin affinity and specificity for Kindlin-3 is likely due to a conformational change in either β1-integrin or Kindlin-3. To identify regions that underwent significant conformational changes during the Q595P mutation simulation, we used the Bio3D package to locate the rigid structural core of the Kindlin-3/β1-integrin complex. The results indicated that the WT complex retained a well-defined and stable core with minimal conformational changes (Figure 3A). In contrast, the Q595P mutant system showed reduced stability (Figure 3B), as evidenced by poor overlap in the α1-α2 loop of Kindlin-3 (residues Thr639-Asp649). This suggested substantial conformational changes in these regions, with β1-integrin trending toward an "inward" conformation. The centroid distance (DMC) between the β1-integrin loop and the α1-α2 loop of Kindlin-3 suggested that the Q595P mutation caused the β1-integrin loop and the α1-α2 loop of Kindlin-3 to move closer (Figure 3C,D). We observed that the angle (θ) between the β1-integrin sheet and the α2 helix and the angle (γ) related to the β5 sheet of Kindlin-3 decreased (Figure 3C,E) and increased (Figure 3C,F), respectively, following induction of the Q595P mutation. This suggests that after the mutation, the β1-integrin sheet shifts toward the α1−α2 helix and away from the β5 sheet, which is a crucial binding site for the interaction between Kindlin-3 and β integrin.[9,10] Overall, these secondary

https://doi.org/10.1021/acsomega.4c10930
ACS Omega 2025, 10, 16396−16409

structural alterations result in the repositioning of the β1-integrin away from its conventional binding interface with Kindlin-3. Since previous findings indicated enhanced hydrophobic interactions after the Q595P mutation, we further investigated whether the proximity between the β1-integrin loop and the α1−α2 loop of Kindlin-3 was a result of stronger hydrophobic interactions. We quantified the buried-SASAs between the β1-integrin loop and the α1-α2 loop of Kindlin-3 (Figure 3G). The results showed an increase in buried-SASA after mutation, indicating enhanced hydrophobic interactions.

Q595P Mutation Decreased the Number of H-Bond Interactions at the Binding Interface and Enhanced Hydrophobic Interactions between Nonbinding Surfaces. Interactions between residues at the binding interface are crucial to complex stability. To identify the key residues involved in the observed conformational changes, we examined the H-bond network at the binding interface between the WT and Q595P mutant systems (Table 2). To better understand

Table 2. Hydrogen Interactions in the WT and Q595P Mutant Systems[a]

			H-bond occupancy	
no	Kindlin-3	β1-integrin	WT	Q595P
1	Trp596	Val790	0.97 ± 0.00	0.89 ± 0.03
2	Val598	Thr788	0.95 ± 0.00	0.91 ± 0.06
3	Met593	Asn792	0.89 ± 0.01	0.75 ± 0.09
4	Arg594	Asn792	0.88 ± 0.02	0.00 ± 0.00
5	Ser591	Glu796	0.79 ± 0.04	0.61 ± 0.09
6	Asp610	Tyr795	0.67 ± 0.03	0.56 ± 0.11
7	Asn597	Thr789	0.38 ± 0.07	0.32 ± 0.03
8	Trp600	Val787	0.31 ± 0.04	0.18 ± 0.15
9	Ser638	Lys794	0.27 ± 0.19	0.14 ± 0.11
10	Trp600	Thr788	0.19 ± 0.12	0.12 ± 0.03
11	Ser591	Gly797	0.16 ± 0.04	0.00 ± 0.00
12	Asn597	Thr788	0.11 ± 0.08	0.08 ± 0.03
13	Asp610	Gly797	0.10 ± 0.01	0.00 ± 0.02
14	Glu641	Asn794	0.09 ± 0.09	0.00 ± 0.06
15	Arg644	Glu796	0.07 ± 0.12	0.00 ± 0.03
16	Arg644	Asn794	0.00 ± 0.00	0.15 ± 0.26

[a]Note: all data shown are means ± SD, n = 3.

the binding interfaces, the key residues involved in the interaction between Kindlin-3 and β1-integrin were visualized using a three-dimensional heatmap. A heat map was generated by mapping the data onto a structural model (Figure 4A). The heatmap shows that the binding site of Kindlin-3 may consist of two discontinuous parts. The critical subsite was the β5 sheet of Kindlin-3 (residues Gln595−Asn599) interacting with the β1-integrin sheet (residues Val787−Val791), and the minor subsite was the β4−β5 loop of Kindlin-3 with the initial residues of the β5 sheet (Phe590−Arg594) and β1-integrin loop (Asn792−Gly797). These regions involved in interactions with β1-integrin are termed the sheet-binding site (Figure 4A up) and the loop-binding site (Figure 4A down). The residue pairs Trp596−Val790 (H-bond occupancy of 0.97) and Val598−Thr788 (H-bond occupancy of 0.95) were crucial for the stability of the sheet-binding site (Table 2). The loop regions of proteins typically exhibit high instability. Met593 and Arg594 formed strong hydrogen bonds with Asn792, stabilizing both the beginning of the loop-binding site and the terminal end of the sheet-binding site. Asp610 and Ser591 formed relatively strong hydrogen bonds with Tyr795 and Glu796, respectively, thereby stabilizing the terminal end of the loop-binding site of β1-integrin. The results of the hydrogen bonds demonstrate the importance of the NPXY motif (residues Asn792−Tyr795) on the loop of β1-integrin and the TTV/STF motif (residues Thr788−Val790) on the sheet of β1-integrin in binding with Kindlin-3.[10,11] Almost all strong hydrogen bonding events were weakened in the Q595P mutant simulation, particularly the Arg594−Asn792 hydrogen bond, which disappeared after the mutation simulation (Table 2). The 3D heatmap showed that the Q595P mutant had fewer interactions at both subinterface sites, with a notable decrease at the loop-binding site (Figure 4B). This corresponds to the secondary structure analysis, revealing major conformational changes in this region. To identify the residues responsible for the increase in hydrophobic interactions, we measured the hydrophobic interactions between the β1-integrin loop and the α1−α2 loop, as well as the α2 regions of Kindlin-3 (Table S2). The results indicated that in the WT system, strong hydrophobic interactions contribute to binding, particularly from the Leu656 residue of β1-integrin. After the mutation was introduced, the strong hydrophobic interactions intensified, whereas some initially weak interactions transformed into exceedingly strong interactions. For instance, the interactions between Val791 of Kindlin-3 and two α2 helix residues of β1-integrin (Leu652 and Leu656) changed from very weak to extremely strong. Similarly, the hydrophobic interactions between two residues (Ala643, Leu648) of the Kindlin-3 α1−α2 loop and Pro793 in β1-integrin exhibited marked enhancement (Figure 4C). These results indicated that the Q595P mutation disrupted the stabilization of H-bonds at the interface. As a result, the β1-integrin loop shifted away from the interface, driven by existing hydrophobic interactions, and moved closer to the Kindlin-3 α1−α2 loop.

Q595P Mutation Induced Torsional Angle Changes in Kindlin-3 Interface Residues, Reducing H-Bond Formation with β1-Integrin. To further investigate the effects of the Q595P mutation on these interactions, we focused on the mutated residue Gln595, which is located at the binding interface (Figure 5A). However, interaction assessments of the interface residues (Table 2) indicated that Kindlin-3 Gln595 was not essential for maintaining interface stability. The occupancy of H-bonds of Kindlin-3 Gln595 was only 0.03 in the WT system and 0 in the Q595P mutant system. This suggested that the observed effects did not arise from the loss of key interactions. Given that the Q595P mutation substitutes hydrophilic glutamine (Gln) (Figure 5A) with hydrophobic proline (Pro; Figure 5B), we hypothesized that this mutation induces conformational changes in nearby residues that are essential for stabilizing the interface, thereby weakening the interactions. Using the Bio3D package, we calculated the differences in the torsional angles of interface residues between the WT and Q595P mutant systems, which enabled the rapid identification of residues with significant conformational changes (Figure 5C). The results indicated that residues within the Kindlin-3 β5 sheet of the loop-binding site (residues Phe590−Arg594) exhibited substantial torsional shifts, with Kindlin-3 Arg594 displaying the largest conformational change. Residues on the Kindlin-3 sheet-binding side of the interface (Gln595−Asn599) showed smaller torsional shifts. The data indicated that the mutation induced a twisting motion in the β5 sheet of Kindlin-3, leading to changes in the torsion angles of Arg594 (Figure 5D,E), Met593 (Figure 5D,E), and Ser591 (Figure 5F,G) on the loop-binding site compared with those in

https://doi.org/10.1021/acsomega.4c10930
ACS Omega 2025, 10, 16396−16409

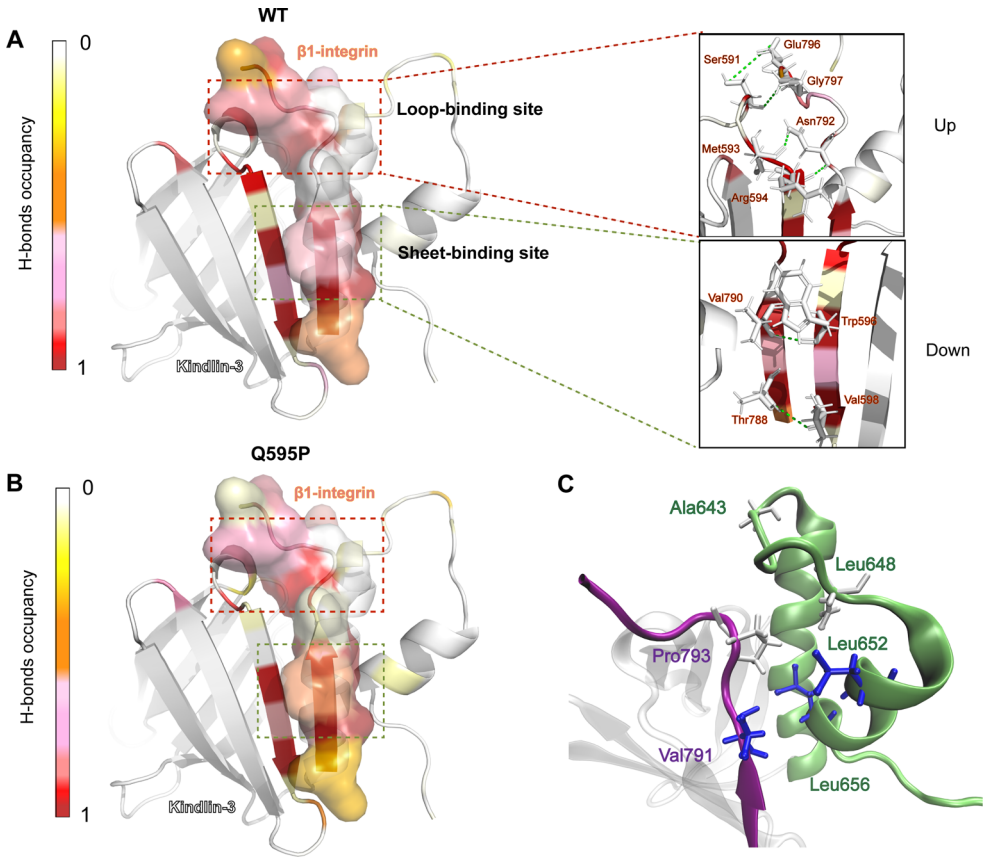

Figure 4. Visualization of H-bonds and hydrophobic interactions. (A) Tridimensional heatmap of H-bond occupancies in the WT system. The residues were color-coded based on occupancy values to highlight the key residues and subdomains. The β1-integrin structure is displayed as a cartoon model with a semitransparent surface, emphasizing the integrin binding sites. (B) Tridimensional heatmap of H-bond occupancies in the Q595P mutant system. (C) Visualization of hydrophobic interaction residues. Val791 and its hydrophobic interaction partners are marked in blue, while Pro793 and its partners are marked in white.

the WT system. After the Kindlin-3 Q595P mutation was introduced, the interaction indices among these residues significantly decreased (Table 2), with the interaction between Arg594 and Asn792 exhibiting the largest torsional shift and disappearing entirely (with the H-bond occupancy dropping from 0.88 to 0). These findings revealed a strong correlation between the torsional shifts and the reduction in the number of interactions among the residues. By calculating the Gaussian distribution of the centroid distances of Arg594−Asn792 (Figure 5H), Met593−Asn792 (Figure 5I), Ser591−Glu796 (Figure 5J), and Ser591−Gly797 (Figure 5K), we found that the Q595P mutation increased the distance between these residue pairs. Consequently, this led to a decrease in the level or complete loss of stabilizing H-bond interactions at the interface.

Q595P Mutation Decreased the Mechanical Strength of the Kindlin-3/β1-Integrin Complex. Kindlin-3 is a mechanosensitive protein that is essential for mechanochemical signal transduction under physiological conditions. The bond between Kindlin-3 and β1-integrin requires a strong mechanical strength. To examine the conformational changes and rupture forces in the Kindlin-3/β1-integrin complex under physiological mechanical conditions, we performed three force-ramp SMD simulations for 50 ns. The force−time curves from the three runs showed that in the WT system, the force profile gradually increased during the first 20 ns (Figure 6A), corresponding to the first plateau in the buried-SASA values (Figure 6C). The force then peaked, decreased sharply, and gradually increased to a second peak at approximately 40 ns, corresponding to the second buried-SASA plateau. The complex fully dissociated at 42.33 ± 2.38 ns, and the level of buried-SASA dropped to 0 (Figure 6C). Conversely, in the Q595P mutant system, the force profile exhibited significant fluctuations across the three simulation runs, with several minor and two prominent peaks, the first of which was notably reduced. The average dissociation time was shorter, at 37.08 ± 4.46 ns (Figure 6B,D). Statistical analysis of the three simulation runs showed that the Q595P mutant system had a reduced average dissociation-rupture force (Figure 6E), an earlier average dissociation-rupture time (Figure 6F), and a significant decrease in stress accumulation (Figure 6G).

To identify the primary residue interactions that counteract the mechanical forces, we analyzed the survival rates of H-bonds at the binding interface of the WT and Q595P mutant systems during stretching. In the WT system, the Kindlin-3-β1-integrin residue pairs Ser591−Glu796, Asp610−Tyr795, Ser638−Asn-794, Arg594−Asn792, and Met593−Asn792 at the loop-binding site remained stable during stretching, contributing significantly to the stability of the binding interface under mechanical force. The residue pairs Trp600−Val787, Asn597−Thr788, Val598−Thr788, Trp600−Thr788, Asn597−Thr789, and Trp596−Val790 dissociated at approximately 20 ns, coinciding with the first peak. These pairs are critical for maintaining mechanical stability at the sheet-

https://doi.org/10.1021/acsomega.4c10930
ACS Omega 2025, 10, 16396−16409

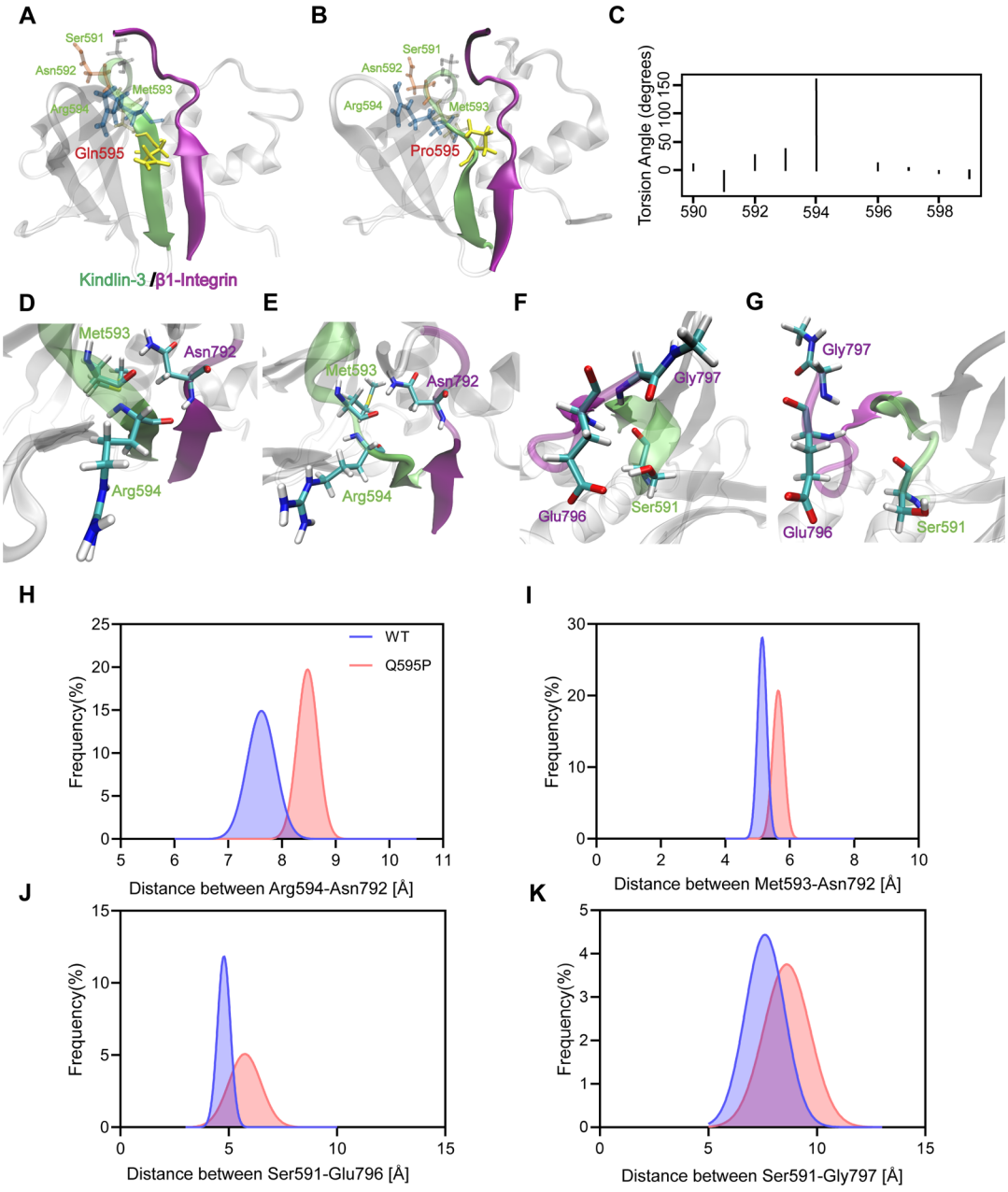

Figure 5. Structural basis of the mutation-induced reduction in binding affinity. (A,B) Diagrams of the Kindlin-3 residue Gln595/Pro595 and adjacent stable interface residues in the WT system (A) and in the Q595P mutant system (B). The integrin is depicted in purple, and the Kindlin-3 binding interface is shown in lime. (C) Differences in the residue torsion angle of the Kindlin-3 binding interface between the WT and Q595P mutant systems. (D,E) Diagrams of the torsion angle of Kindlin-3 Met593 and Arg594 with their residue binding partners on β1-integrin in the WT system (D) and Q595P mutant system (E). (F,G) Diagrams of the torsion angle of Kindlin-3 Ser591 with its paired binding residues on β1-integrin in the WT system (F) and Q595P mutant system (G). (H–K) Gaussian distribution of C_α distances for Arg594–Asn792(H), Met593–Asn792(I), Ser591–Glu796(J), and Ser591–Gly797(K) in the WT and Q595P mutant systems.

binding site. The residue pairs Glu641–Asn794 and Thr639–Asn794 only appeared during the later stages of stretching, suggesting that these H-bonds may be involved in the force-regulating mechanisms of the Kindlin-3/β1-integrin complex (Figure 7A). In the Q595P mutant system, H-bond analysis revealed a reduction in both the number and survival rates of H-bonds during stretching compared to those of the WT system (Figure 7B). Arg594–Asn792 disappeared under stress, and the interaction strength of Met593–Asn792 decreased significantly. These interactions are crucial for maintaining the contact interface under mechanical forces in WT systems. The dissociation pathways showed distinct conformational differences between the WT and Q595P mutant systems. In the WT system, the β1 sheet separated at 19 ns but both binding sites remained stable (Figure 7C). In contrast, in the Q595P mutant system, the β1 sheet remained stable until the later phase of stretching at 24.64 ns when separation occurred (Figure 7D). The results of the analysis of H-bonds and conformational changes during stretching highlighted the reduction in the mechanical strength after mutation.

https://doi.org/10.1021/acsomega.4c10930
ACS Omega 2025, 10, 16396–16409

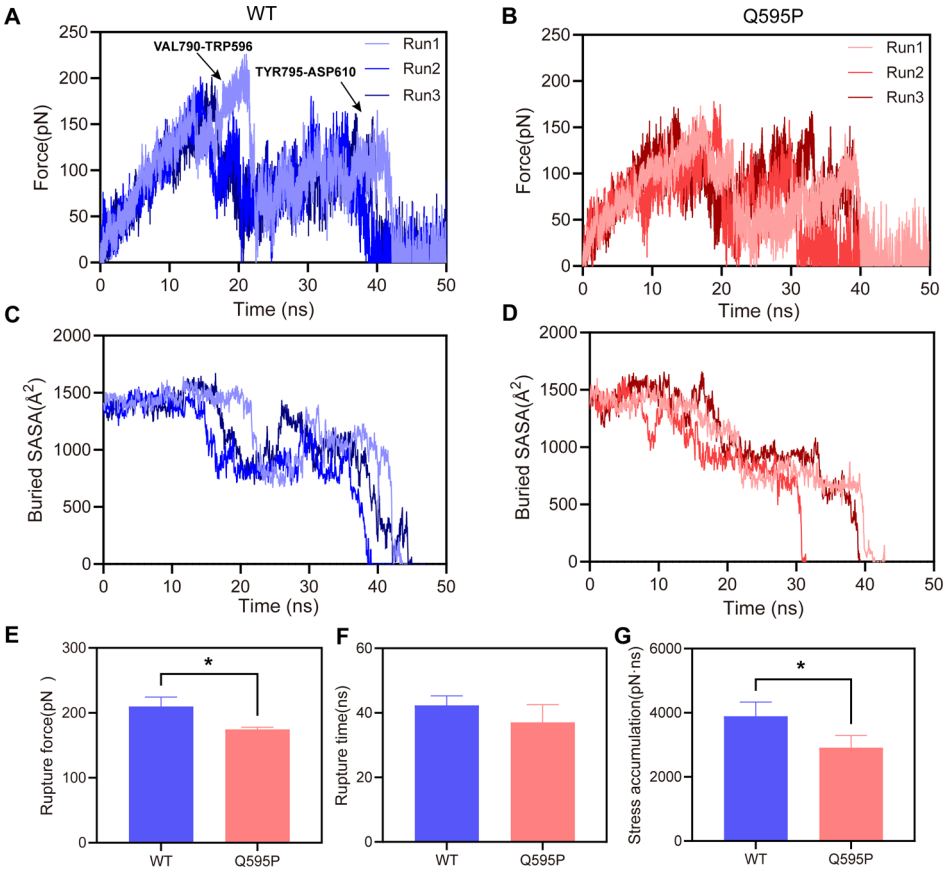

Figure 6. Mechanical stability of the WT and Q595P mutant systems. (A,B) Force spectrum curves from three simulations of the WT system (A) and the Q595P mutant system (B). In the WT system, the rupture of the Trp596−Val790 hydrogen bond was associated with the separation of the sheet interface, while the Asp610−Tyr795 hydrogen bond rupture corresponded to loop interface separation, as indicated by black arrows. (C,D) Changes in buried-SASA values over time during stretching in the WT system (C) and the Q595P mutant system (D) based on three runs. (E) Rupture forces, (F) rupture times, and (G) accumulated stress in the WT and Q595P mutant systems from three runs. For the WT system, the rupture force, rupture time, and accumulated stress reached 209.91 ± 11.83 pN, 42.33 ± 2.61 ns, and 3892.24 ± 337.15 pN·ns, respectively, which were higher than those of the Q595P mutant system (174.995 ± 2.56 pN, 37.41 ± 4.97 ns, 2787.33 ± 311.09 pN·ns). Statistical significance was indicated by $p < 0.05$ (*) based on unpaired two-tailed Student's t test. All data shown are means ± SD, $n = 3$.

DISCUSSION

Kindlins are critical mediators of integrin activation, playing essential roles in diverse physiological and pathological processes including immune responses, cell adhesion, and signal transduction. Mutations in Kindlin-3 cause LAD-III, with the Q595P mutation being particularly notable. Located within the conserved QW motif, this mutation is critical for integrin binding.[11,27] Loss of this site prevents Kindlins from localizing to focal adhesions and impairs integrin activation.[49] ITC analysis demonstrates that this mutation disrupts the binding affinity between Kindlins and integrins.[11] Gln595 situated on the F3 domain binding surface does not form stable interactions with β-integrins yet still leads to severe consequences. While macro-level studies have extensively explored these interactions, the atomic-level mechanisms by which single-residue mutations disrupt them remain unclear, motivating our investigation into the underlying molecular mechanisms. This study utilized MD and SMD simulations to elucidate the molecular mechanism underlying the Q595P mutation of Kindlin-3, a mutation known to cause LAD-III. Our findings not only provide detailed insights into this specific mutation but also establish a molecular framework for understanding how hydrophobicity-driven mutations in Kindlin proteins affect integrin-related functions across a broad spectrum of diseases.

Complex formation stability is maintained through various interactions, including hydrogen bonds (H-bonds), van der Waals forces, and hydrophobic interactions.[50,51] Hydrogen bonds play a dominant role in short-range binding and the formation of a stable interface, which are crucial for protein−ligand recognition and binding. In contrast, hydrophobic effects, although less specific, are the key driving forces of binding.[52] Our findings indicate that the Kindlin-3 Q595P mutation reduces the hydrogen bonds at the interface in the Kindlin-3/β1-integrin complex, while slightly increasing hydrophobic interactions, suggesting a decrease in interaction specificity. The MMPBSA results demonstrated an increase in the binding free energy after the mutation. Therefore, although hydrophobic interactions at the binding interface increase, they do not compensate for the loss of other critical specific interactions, leading to decreased binding affinity and specificity of the Kindlin-3/β1-integrin complex due to the Q595P mutation.

The increase in the RMSD values for monomers and the Kindlin-3/β1-integrin complex after the Q595P mutation suggests that changes in binding affinity and specificity are likely related to conformational changes induced by the

https://doi.org/10.1021/acsomega.4c10930
ACS Omega 2025, 10, 16396−16409

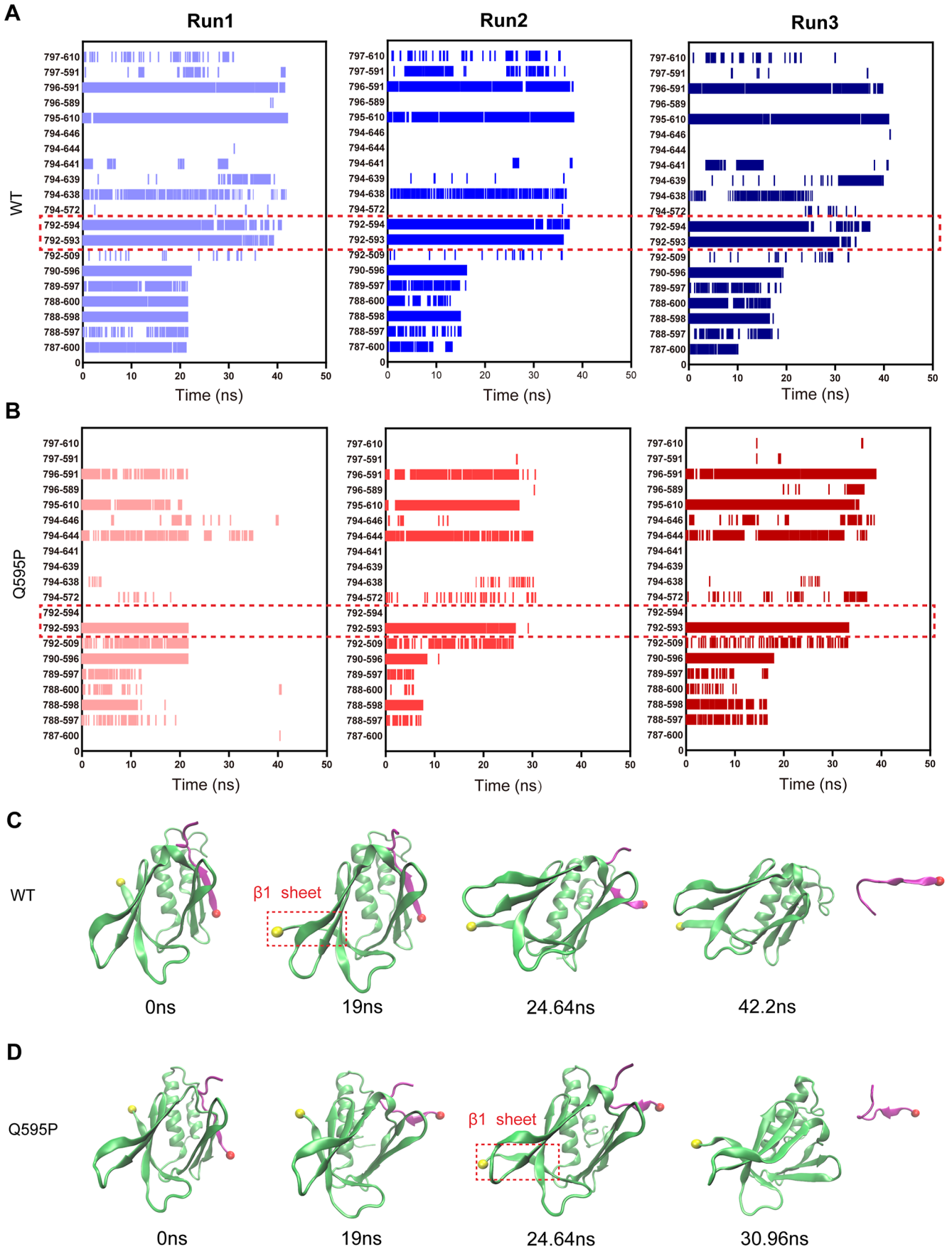

Figure 7. H-bond occupancy and force-induced allostery with changes in pulling time. (A,B) Occupancy patterns of H-bonds across the complex interface from three simulations of the WT system (A) and the Q595P mutant system (B). Key residue pairs affected by the mutation are highlighted in red dashed boxes. (C,D) Typical snapshots of four intermediate complexes at different simulation times for the WT system (C) and

https://doi.org/10.1021/acsomega.4c10930
ACS Omega 2025, 10, 16396−16409

Figure 7. continued

Q595P mutant system (D). Results of the first run of the WT system and the second run of the Q595P mutant system. Distinct conformational changes during stretching are indicated by the time when the β1 sheet detaches.

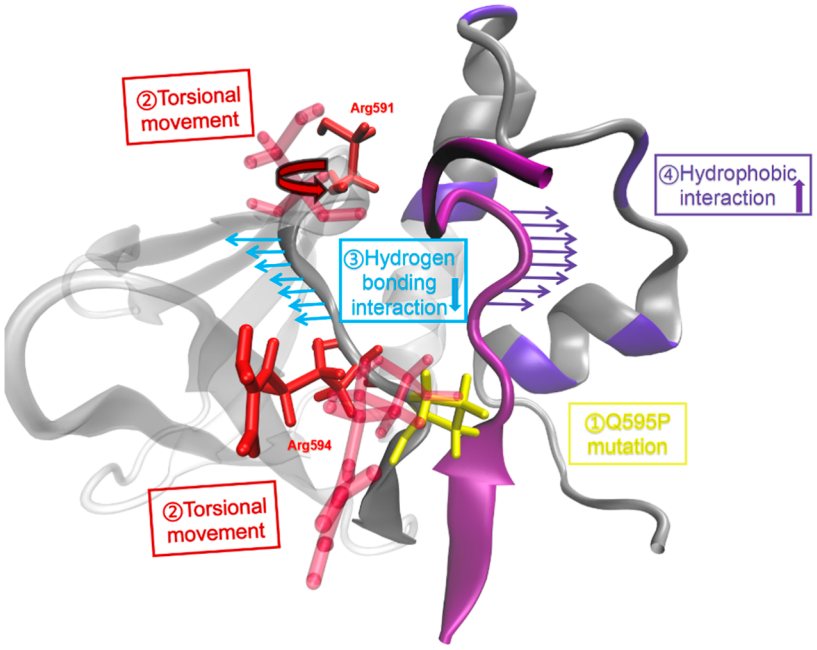

Figure 8. Schematic mechanism of impaired integrin activation caused by the Q595P mutation.

mutation (Figure 1). Principal component analysis revealed that, after the Kindlin-3 Q595P mutation, the β1-integrin is displaced from the binding interface and embedded deeper within the hydrophobic core. The β1-integrin loop region and the α1-α2 loop of Kindlin-3 undergo significant conformational changes. The increase in the buried-SASA values and decrease in the centroid distance suggest closer proximity, likely due to the enhancement of hydrophobic interactions. However, the angle between the β1-integrin sheet region and the α2 helix of Kindlin-3 decreased after the mutation was introduced, whereas the angle with the β5 sheet increased. This indicated that the integrin sheet structure shifted away from the β5 sheet binding interface and toward helix α2 (Figure 3). Previous studies have suggested that the α1-α2 loop is located at the interaction interface between the F3 and F1 domains, where residues such as Arg640 form salt bridges with the Glu137 and Glu138 residues on the F1 domain, maintaining a compact cloverleaf conformation crucial for integrin activation.[53] Mutations in these critical residues, such as the E138K mutation found in LAD III cases,[21] emphasize the importance of this compact conformation in integrin activation. Our results indicated that after the Q595P mutation, the α1−α2 loop underwent significant conformational changes, bringing it closer to the β1-integrin loop region. We hypothesized that these changes disrupt its interactions with the Kindlin-3 F1 domain, affecting its compact structure and leading to abnormal integrin activation, but this hypothesis warrants further investigation.

Alterations in the secondary structure reflect changes in the primary molecular structure. The Q595P mutation decreased the hydrogen bond interactions at both subbinding sites, particularly at the loop-binding site, leading to the loss of the high-interaction Arg594−Asn792 residue pair (Figure 4). Torsional angle analysis revealed that the Kindlin-3 residues at the loop-binding site underwent greater torsional shifts than those at the sheet-binding site, with Arg594 showing the most significant shifts (Figure 5). This suggests that the reduced hydrogen bond interactions resulted from torsional shifts, and the extent of these shifts correlates with the reduction in interactions. Consequently, stabilizing residues such as Arg594, Met593, and Ser591 undergo varying degrees of twisting, increasing their distance from paired residues and diminishing or eliminating hydrogen-bond interactions. In the WT, Kindlin-3 residues Iie635 and Leu656 are essential for maintaining the hydrophobic environment that supports binding, which is consistent with previous experimental findings.[11] The Q595P mutation increases the number of residues that exhibit a strong hydrophobicity. The reduction in the number of hydrogen bond interactions led to instability at the interface, causing β1-integrin to be predominantly influenced by its hydrophobic interactions with Kindlin-3, thereby shifting further from the binding interface.

Kindlin-3 is a force-sensitive protein capable of transmitting mechanical signals from actin,[54] requiring sufficient mechanical strength to ensure the stability and efficacy of mechanical signal transduction. Additional studies have further demonstrated the crucial role of Kindlin-3 in supporting talin-mediated integrin activation.[37] Our SMD simulation results showed that the WT complex can withstand a peak force of 209.9 ± 14.5 pN, indicating a high mechanical strength. However, after the Q595P mutation was introduced, this value decreased to 174.6 ± 3.1 pN, resulting in premature rupture and reduced stress accumulation, thereby diminishing the mechanical strength of the complex. Due to inherent time scale effects in the simulation, the rupture forces observed were higher than those recorded experimentally, meaning that

https://doi.org/10.1021/acsomega.4c10930
ACS Omega 2025, 10, 16396−16409

simulation results typically cannot be directly compared with experimental data. However, Posch et al. demonstrated that there is qualitative consistency between the simulation data and single-molecule experimental data.[55,56] Therefore, the observed phenomena still provide valuable predictions for understanding physiological structures and biological functions. Analysis of hydrogen bond interactions during stretching revealed that the residues significantly contributed to the complex stability under force conditions. In the WT system, the high occupancy of the Asn792−Arg594 residue pair during equilibrium and stretching indicated its critical role in maintaining complex integrity under both forceful and nonforceful conditions. However, this interaction was lost after the mutation was induced. Therefore, the Q595P mutation not only reduced the binding affinity and specificity but also weakened the mechanical stability of the complex.

CONCLUSIONS

In summary, this study elucidates the molecular mechanism by which the Kindlin-3 Q595P mutation disrupts integrin binding and activation, emphasizing the critical role of hydrophobicity and hydrogen bond dynamics in maintaining interaction stability(Figure 8). Gln595 is located within the binding site of Kindlin-3 F3 but does not directly form hydrogen bonds to stabilize the binding interface. The mutation induced a shift from hydrophilic to hydrophobic properties, altering the regional characteristics. The introduced hydrophobic proline (Pro) residue avoids the aqueous environment, causing torsional shifts in adjacent residues, such as Arg594 and Ser591. These shifts disrupt essential interactions at the binding interface, displacing β1-integrin from its site. Additional hydrophobic interactions enhanced this displacement, ultimately reducing the binding affinity and specificity. The residues affected by torsional shifts and reduced hydrogen bonding also contributed to the mechanical stability of the complex. These structural alterations reduce the resilience of the complex to mechanical stress, thereby reducing its overall strength. These disruptions may have impaired the binding of Kindlin-3 to β1-integrin and mechanotransduction, potentially contributing to disease pathogenesis.

In WT Kindlin-3, residue pairs Arg594−Asn792, Ser591−Glu796, and Ser591−Gly797 within the loop-binding site stabilize the interface. After the Q595P mutation was induced, the hydrophobicity of Kindlin-3 at the binding site changes, caused by torsional movement in the residues Ser591 and Arg594, which disrupts the formation of hydrogen bonds with β1-integrin. This disruption moves integrin away from the hydrogen bond-maintained interface and closer to the nonbinding interface through enhanced hydrophobic interactions. As a result, these changes reduce the mechanical stability of the complex, making Kindlin-3 more susceptible to dissociation. The Q595P-mutated residue is highlighted in yellow, and residues Ser591 and Arg594 are depicted in red. The WT residues are shown semitransparently. Blue arrows indicate hydrogen bond disruption, while violet arrows and purple segments in the structure represent enhanced hydrophobic interactions and major hydrophobic patches, respectively.

ASSOCIATED CONTENT

Data Availability Statement

The crystal structure used in this study is available from the Protein Data Bank (PDB) with IDs: 6V9G and 5XQ0. The MD simulations were performed using VMD (version 1.9.3) for visualization, available at https://www.ks.uiuc.edu/Research/vmd/, and NAMD (version 2.14) for the simulations, available at https://www.ks.uiuc.edu/Research/namd/. PyMOL (version 2.6.0) was used for additional structural analysis and can be accessed at https://pymol.org/2/. The CHARMM36 force field used in the simulations was obtained from the official CHARMM Web site, https://www.charmm.org/. For data analysis, the Bio3D (version 2.4) package was used, and more information can be found at http://thegrantlab.org/bio3d/. All scripts, configuration files, and relevant input and output files used for the simulations are available at Zenodo with DOI 10.5281/zenodo.14203558.

Supporting Information

The Supporting Information is available free of charge at https://pubs.acs.org/doi/10.1021/acsomega.4c10930.

Conceptual framework of this work; exploration of constant velocity stretching parameters; time profile of radius of gyration and buried-SASA values; RMSD, buried-SASA, and N_{HB} for three runs; $Q-Q$ plots of the two systems; hydrogen bond interactions in the 5XQ0 complex; and hydrophobic interactions in the WT and Q595P systems (PDF)

AUTHOR INFORMATION

Corresponding Authors

Quhuan Li − *School of Bioscience and Bioengineering, South China University of Technology, Guangzhou 510006, China*; Email: liqh@scut.edu.cn

Fengxia Zhang − *Department of Nephrology, First Affiliated Hospital of Gannan Medical University, Ganzhou, Jiangxi province 341000, China*; orcid.org/0009-0001-9538-1402; Email: zhangfengxia@gmu.cn

Author

Xianwen Luo − *School of Bioscience and Bioengineering, South China University of Technology, Guangzhou 510006, China*

Complete contact information is available at: https://pubs.acs.org/10.1021/acsomega.4c10930

Author Contributions

W.L and Q.L. designed this research; W.L. overall performed research and analyzed data; and W.L., Q.L., and F.Z. wrote this paper.

Funding

This work was funded by the National Natural Science Foundation of China (31870928 and 32271360), the Natural Science Foundation of Guangdong Province, China (2021A1515010040 and 2023A1515010829), the Jiangxi Province Natural Science Foundation Project (20242BAB25448), the Jiangxi Provincial Department of Science and Technology (202130649), and the First Affiliated Hospital of Gannan Medical University's Hospital level Science and Technology Plan (YJZD202010).

Notes

The authors declare no competing financial interest.

ACKNOWLEDGMENTS

The authors thank Xubin Xie for his help in data treatment of this work.

REFERENCES

(1) Mitroulis, I.; Alexaki, V. I.; Kourtzelis, I.; Ziogas, A.; Hajishengallis, G.; Chavakis, T. Leukocyte integrins: role in leukocyte recruitment and as therapeutic targets in inflammatory disease. *Pharmacol. Ther.* **2015**, *147*, 123−135.

(2) Ou, Z.; Dolmatova, E.; Lassègue, B.; Griendling, K. K. β1- and β2-integrins: central players in regulating vascular permeability and leukocyte recruitment during acute inflammation. *Am. J. Physiol. Heart Circ. Physiol.* **2021**, *320* (2), H734−h739.

(3) Park, E. J.; Myint, P. K.; Ito, A.; Appiah, M. G.; Darkwah, S.; Kawamoto, E.; Shimaoka, M. Integrin-ligand interactions in inflammation, cancer, and metabolic disease: insights into the multifaceted roles of an emerging ligand irisin. *Front. Cell Dev. Biol.* **2020**, *8*, 588066.

(4) Rognoni, E.; Ruppert, R.; Fässler, R. The kindlin family: functions, signaling properties and implications for human disease. *J. Cell Sci.* **2016**, *129* (1), 17−27.

(5) Wang, H.; Wang, C.; Long, Q.; Zhang, Y.; Wang, M.; Liu, J.; Qi, X.; Cai, D.; Lu, G.; Sun, J.; et al. Kindlin2 regulates neural crest specification via integrin-independent regulation of the FGF signaling pathway. *Development* **2021**, *148* (10), dev199441.

(6) Lai-Cheong, J. E.; Parsons, M.; McGrath, J. A. The role of kindlins in cell biology and relevance to human disease. *Int. J. Biochem. Cell Biol.* **2010**, *42* (5), 595−603.

(7) Larjava, H.; Plow, E. F.; Wu, C. Kindlins: essential regulators of integrin signalling and cell-matrix adhesion. *EMBO Rep.* **2008**, *9* (12), 1203−1208.

(8) Goult, B. T.; Bouaouina, M.; Harburger, D. S.; Bate, N.; Patel, B.; Anthis, N. J.; Campbell, I. D.; Calderwood, D. A.; Barsukov, I. L.; Roberts, G. C.; et al. The structure of the N-terminus of kindlin-1: a domain important for alphaiibbeta3 integrin activation. *J. Mol. Biol.* **2009**, *394* (5), 944−956.

(9) Bu, W.; Levitskaya, Z.; Loh, Z. Y.; Jin, S.; Basu, S.; Ero, R.; Yan, X.; Wang, M.; Ngan, S. F. C.; Sze, S. K.; et al. Structural basis of human full-length kindlin-3 homotrimer in an auto-inhibited state. *PLoS Biol.* **2020**, *18* (7), No. e3000755.

(10) Harburger, D. S.; Bouaouina, M.; Calderwood, D. A. Kindlin-1 and −2 directly bind the C-terminal region of beta integrin cytoplasmic tails and exert integrin-specific activation effects. *J. Biol. Chem.* **2009**, *284* (17), 11485−11497.

(11) Li, H.; Deng, Y.; Sun, K.; Yang, H.; Liu, J.; Wang, M.; Zhang, Z.; Lin, J.; Wu, C.; Wei, Z.; et al. Structural basis of kindlin-mediated integrin recognition and activation. *Proc. Natl. Acad. Sci. U. S. A* **2017**, *114* (35), 9349−9354.

(12) Aretz, J.; Aziz, M.; Strohmeyer, N.; Sattler, M.; Fässler, R. Talin and kindlin use integrin tail allostery and direct binding to activate integrins. *Nat. Struct. Mol. Biol.* **2023**, *30* (12), 1913−1924.

(13) Bu, W.; Levitskaya, Z.; Tan, S. M.; Gao, Y. G. Emerging evidence for kindlin oligomerization and its role in regulating kindlin function. *J. Cell Sci.* **2021**, *134* (8), jcs256115.

(14) Ussar, S.; Wang, H. V.; Linder, S.; Fässler, R.; Moser, M. The Kindlins: subcellular localization and expression during murine development. *Exp. Cell Res.* **2006**, *312* (16), 3142−3151.

(15) Qu, H.; Tu, Y.; Shi, X.; Larjava, H.; Saleem, M. A.; Shattil, S. J.; Fukuda, K.; Qin, J.; Kretzler, M.; Wu, C. Kindlin-2 regulates podocyte adhesion and fibronectin matrix deposition through interactions with phosphoinositides and integrins. *J. Cell Sci.* **2011**, *124* (6), 879−891.

(16) Huet-Calderwood, C.; Brahme, N. N.; Kumar, N.; Stiegler, A. L.; Raghavan, S.; Boggon, T. J.; Calderwood, D. A. Differences in binding to the ILK complex determines kindlin isoform adhesion localization and integrin activation. *J. Cell Sci.* **2014**, *127* (Pt 19), 4308−4321.

(17) Lai-Cheong, J. E.; Tanaka, A.; Hawche, G.; Emanuel, P.; Maari, C.; Taskesen, M.; Akdeniz, S.; Liu, L.; McGrath, J. A. Kindler syndrome: a focal adhesion genodermatosis. *Br. J. Dermatol.* **2009**, *160* (2), 233−242.

(18) Zhang, Q.; Yang, Q.; Shen, F.; Wang, L.; Luo, J. Identification of a novel FERMT1 variant causing kindler syndrome and a review of the clinical and molecular genetic features in Chinese patients. *Front Pediatr* **2024**, *12*, 1425030.

(19) Yahya, A. M.; AlMulla, A. A.; AlRufaye, H. J.; Al Dhaheri, A.; Elomami, A. S.; Al-Hammadi, S.; Kailas, L.; Vijayan, R.; Souid, A. K. Case report: a case of leukocyte adhesion deficiency, type III presenting with impaired platelet function, lymphocytosis and granulocytosis. *Front Pediatr* **2021**, *9*, 713921.

(20) Köker, N.; Deveci, I.·.; van Leeuwen, K.; Akbayram, S.; Roos, D.; Kuijpers, T. W.; Köker, M. Y. A novel deletion in FERMT3 causes LAD-III in a turkish family. *J. Clin. Immunol.* **2023**, *43* (4), 741−746.

(21) Xu, Z.; Jobe, S. M.; Ma, Y. Q.; Shavit, J. A. A novel leukocyte adhesion deficiency type III mutation manifests functional importance of the compact FERM domain in kindlin-3. *J. Thromb. Hemost.* **2024**, *22* (2), 558−564.

(22) Fagerholm, S. C.; Lek, H. S.; Morrison, V. L. Kindlin-3 in the immune system. *Afr. J. Clin. Exp. Immunol.* **2014**, *27* (1), 37−42.

(23) Mory, A.; Feigelson, S. W.; Yarali, N.; Kilic, S. S.; Bayhan, G. I.; Gershoni-Baruch, R.; Etzioni, A.; Alon, R. Kindlin-3: a new gene involved in the pathogenesis of LAD-III. *Blood* **2008**, *112* (6), 2591.

(24) Svensson, L.; Howarth, K.; McDowall, A.; Patzak, I.; Evans, R.; Ussar, S.; Moser, M.; Metin, A.; Fried, M.; Tomlinson, I.; et al. Leukocyte adhesion deficiency-III is caused by mutations in KINDLIN3 affecting integrin activation. *Nat. Med.* **2009**, *15* (3), 306−312.

(25) Suratannon, N.; Yeetong, P.; Srichomthong, C.; Amarinthnukrowh, P.; Chatchatee, P.; Sosothikul, D.; van Hagen, P. M.; van der Burg, M.; Wentink, M.; Driessen, G. J.; et al. Adaptive immune defects in a patient with leukocyte adhesion deficiency type III with a novel mutation in FERMT3. *Pediatr. Allergy Immunol.* **2016**, *27* (2), 214−217.

(26) Has, C.; Castiglia, D.; del Rio, M.; Diez, M. G.; Piccinni, E.; Kiritsi, D.; Kohlhase, J.; Itin, P.; Martin, L.; Fischer, J.; et al. Kindler syndrome: extension of FERMT1 mutational spectrum and natural history. *Hum. Mutat.* **2011**, *32* (11), 1204−1212.

(27) Shi, X.; Ma, Y. Q.; Tu, Y.; Chen, K.; Wu, S.; Fukuda, K.; Qin, J.; Plow, E. F.; Wu, C. The MIG-2/integrin interaction strengthens cell-matrix adhesion and modulates cell motility. *J. Biol. Chem.* **2007**, *282* (28), 20455−20466.

(28) Bledzka, K.; Bialkowska, K.; Sossey-Alaoui, K.; Vaynberg, J.; Pluskota, E.; Qin, J.; Plow, E. F. Kindlin-2 directly binds actin and regulates integrin outside-in signaling. *J. Cell Biol.* **2016**, *213* (1), 97−108.

(29) Alonso, H.; Bliznyuk, A. A.; Gready, J. E. Combining docking and molecular dynamic simulations in drug design. *Med. Res. Rev.* **2006**, *26* (5), 531−568.

(30) Amir, M.; Ahamad, S.; Mohammad, T.; Jairajpuri, D. S.; Hasan, G. M.; Dohare, R.; Islam, A.; Ahmad, F.; Hassan, M. I. Investigation of conformational dynamics of Tyr89Cys mutation in protection of telomeres 1 gene associated with familial melanoma. *J. Biomol. Struct. Dyn.* **2021**, *39* (1), 35−44.

(31) Hsin, J.; Arkhipov, A.; Yin, Y.; Stone, J. E.; Schulten, K. Using VMD: an introductory tutorial. *Curr. Protoc. Bioinf.* **2008**, *24*, 5.

(32) Giorgino, T. Analysis libraries for molecular trajectories: a cross-language synopsis. *Methods Mol. Biol.* **2019**, *2022*, 503−527.

(33) Honorato, R. V.; Trellet, M. E.; Jiménez-García, B.; Schaarschmidt, J. J.; Giulini, M.; Reys, V.; Koukos, P. I.; Rodrigues, J.; Karaca, E.; van Zundert, G. C. P.; et al. The HADDOCK2.4 web server for integrative modeling of biomolecular complexes. *Nat. Protoc.* **2024**, *19* (11), 3219−3241.

(34) Phillips, J. C.; Hardy, D. J.; Maia, J. D. C.; Stone, J. E.; Ribeiro, J. V.; Bernardi, R. C.; Buch, R.; Fiorin, G.; Hénin, J.; Jiang, W.; et al. Scalable molecular dynamics on CPU and GPU architectures with NAMD. *J. Chem. Phys.* **2020**, *153* (4), 044130.

(35) Yu, Y.; Klauda, J. B. Update of the CHARMM36 united atom chain model for hydrocarbons and phospholipids. *J. Phys. Chem. B* **2020**, *124* (31), 6797−6812.

(36) Rosignoli, S.; Paiardini, A. Boosting the full potential of PyMOL with structural biology plugins. *Biomolecules* **2022**, *12* (12), 1764.

https://doi.org/10.1021/acsomega.4c10930
ACS Omega 2025, 10, 16396−16409

(37) Ji, Y.; Fang, Y.; Wu, J. Tension enhances the binding affinity of β1 integrin by clamping Talin tightly: an insight from steered molecular dynamics simulations. *J. Chem. Inf. Model.* **2022**, *62* (22), 5688−5698.
(38) Su, S.; Ling, Y.; Fang, Y.; Wu, J. Force-enhanced biophysical connectivity of platelet β3 integrin signaling through talin is predicted by steered molecular dynamics simulations. *Sci. Rep.* **2022**, *12* (1), 4605.
(39) Jiang, X.; Sun, X.; Lin, J.; Ling, Y.; Fang, Y.; Wu, J. MD simulations on a well-built docking model reveal fine mechanical stability and force-dependent dissociation of Mac-1/GPIbα complex. *Front. Mol. Biosci.* **2021**, *8*, 638396.
(40) Heymann, B.; Grubmüller, H. AN02/DNP-hapten unbinding forces studied by molecular dynamics atomic force microscopy simulations. *Chem. Phys. Lett.* **1999**, *303* (1), 1−9.
(41) Zhang, Y.; Lin, Z.; Fang, Y.; Wu, J. Prediction of Catch-Slip Bond Transition of Kindlin2/β3 Integrin via Steered Molecular Dynamics Simulation. *J. Chem. Inf. Model.* **2020**, *60* (10), 5132−5141.
(42) Genheden, S.; Ryde, U. The MM/PBSA and MM/GBSA methods to estimate ligand-binding affinities. *Expet Opin. Drug Discov.* **2015**, *10* (5), 449−461.
(43) Wang, C.; Greene, D.; Xiao, L.; Qi, R.; Luo, R. Recent developments and applications of the MMPBSA method. *Front. Mol. Biosci.* **2018**, *4*, 87.
(44) Pirojsirikul, T.; Lee, V. S.; Nimmanpipug, P. Unraveling bacterial single-stranded sequence specificities: insights from molecular dynamics and MMPBSA analysis of oligonucleotide probes. *Mol. Biotechnol.* **2024**, *66* (4), 582−591.
(45) Swanson, J. M.; Henchman, R. H.; McCammon, J. A. Revisiting free energy calculations: a theoretical connection to MM/PBSA and direct calculation of the association free energy. *Biophys. J.* **2004**, *86* (1), 67−74.
(46) Ganoth, A.; Friedman, R.; Nachliel, E.; Gutman, M. A molecular dynamics study and free energy analysis of complexes between the Mlc1p protein and two IQ motif peptides. *Biophys. J.* **2006**, *91* (7), 2436−2450.
(47) Grant, B. J.; Rodrigues, A. P.; ElSawy, K. M.; McCammon, J. A.; Caves, L. S. Bio3d: an R package for the comparative analysis of protein structures. *Bioinformatics* **2006**, *22* (21), 2695−2696.
(48) Skjærven, L.; Yao, X. Q.; Scarabelli, G.; Grant, B. J. Integrating protein structural dynamics and evolutionary analysis with Bio3D. *BMC Bioinf.* **2014**, *15* (1), 399.
(49) Xu, Z.; Chen, X.; Zhi, H.; Gao, J.; Bialkowska, K.; Byzova, T. V.; Pluskota, E.; White, G. C.; Liu, J.; Plow, E. F.; et al. Direct interaction of kindlin-3 with integrin αIIbβ3 in platelets is required for supporting arterial thrombosis in mice. *Arterioscler. Thromb. Vasc. Biol.* **2014**, *34* (9), 1961−1967.
(50) Janin, J.; Bahadur, R. P.; Chakrabarti, P. Protein-protein interaction and quaternary structure. *Q. Rev. Biophys.* **2008**, *41* (2), 133−180.
(51) Bahadur, R. P.; Chakrabarti, P.; Rodier, F.; Janin, J. A dissection of specific and non-specific protein-protein interfaces. *J. Mol. Biol.* **2004**, *336* (4), 943−955.
(52) Sun, Q. The hydrophobic effects: our current understanding. *Molecules* **2022**, *27* (20), 7009.
(53) Sun, J.; Xiao, D.; Ni, Y.; Zhang, T.; Cao, Z.; Xu, Z.; Nguyen, H.; Zhang, J.; White, G. C.; Ding, J.; et al. Structure basis of the FERM domain of kindlin-3 in supporting integrin αIIbβ3 activation in platelets. *Blood Adv.* **2020**, *4* (13), 3128−3135.
(54) Chen, S.; He, T.; Zhong, Y.; Chen, M.; Yao, Q.; Chen, D.; Shao, Z.; Xiao, G. Roles of focal adhesion proteins in skeleton and diseases. *Acta Pharm. Sin. B* **2023**, *13* (3), 998−1013.
(55) Posch, S.; Aponte-Santamaría, C.; Schwarzl, R.; Karner, A.; Radtke, M.; Gräter, F.; Obser, T.; König, G.; Brehm, M. A.; Gruber, H. J.; et al. Single molecule force spectroscopy data and BD- and MD simulations on the blood protein von Willebrand factor. *Data Brief* **2016**, *8*, 1080−1087.
(56) Posch, S.; Aponte-Santamaría, C.; Schwarzl, R.; Karner, A.; Radtke, M.; Gräter, F.; Obser, T.; König, G.; Brehm, M. A.; Gruber, H. J.; et al. Mutual A domain interactions in the force sensing protein von Willebrand factor. *J. Struct. Biol.* **2017**, *197* (1), 57−64.

https://doi.org/10.1021/acsomega.4c10930
ACS Omega 2025, 10, 16396−16409